AGU PUBLICATIONS

Geophysical Research Letters

RESEARCH LETTER
10.1002/2017GL074691

Conditions leading to the unprecedented low Antarctic sea ice extent during the 2016 austral spring season

Malte F. Stuecker[1,2], Cecilia M. Bitz[1], and Kyle C. Armour[1,3]

[1]Department of Atmospheric Sciences, University of Washington, Seattle, Washington, USA, [2]Cooperative Programs for the Advancement of Earth System Science, University Corporation for Atmospheric Research, Boulder, Colorado, USA, [3]School of Oceanography, University of Washington, Seattle, Washington, USA

Key Points:
- Record low Antarctic sea ice extent in 2016 austral spring can be related to two rare events
- First: anomalously long quasi-stationary persistence of El Niño-induced SST anomalies in the eastern Ross, Amundsen, and Bellingshausen Seas
- Second: unforced SAM variability driving warm SSTs and sea ice decline in most of the remaining Southern Ocean sectors

Supporting Information:
- Supporting Information S1

Correspondence to:
M. F. Stuecker,
stuecker@atmos.washington.edu

Citation:
Stuecker, M. F., C. M. Bitz, and K. C. Armour (2017), Conditions leading to the unprecedented low Antarctic sea ice extent during the 2016 austral spring season, *Geophys. Res. Lett.*, *44*, 9008–9019, doi:10.1002/2017GL074691.

Received 12 APR 2017
Accepted 18 AUG 2017
Accepted article online 24 AUG 2017
Published online 9 SEP 2017

Abstract The 2016 austral spring was characterized by the lowest Southern Hemisphere (SH) sea ice extent seen in the satellite record (1979 to present) and coincided with anomalously warm surface waters surrounding most of Antarctica. We show that two distinct processes contributed to this event: First, the extreme El Niño event peaking in December–February 2015/2016 contributed to pronounced extratropical SH sea surface temperature and sea ice extent anomalies in the eastern Ross, Amundsen, and Bellingshausen Seas that persisted in part until the following 2016 austral spring. Second, internal unforced atmospheric variability of the Southern Annular Mode promoted the exceptional low sea ice extent in November–December 2016. These results suggest that a combination of tropically forced and internal SH atmospheric variability contributed to the unprecedented sea ice decline during the 2016 austral spring, on top of a background of slow changes expected from greenhouse gas and ozone forcing.

1. Introduction

The low Antarctic sea ice extent initiated in austral spring 2016 was truly exceptional [*Turner et al.*, 2017], well exceeding three standard deviations of the observed 1979–2016 ice extent (Figure 1a) and with anomalously low sea ice concentrations everywhere except in some parts of the Ross Sea and Indian Ocean sector (Figure 1c). The low sea ice extent was accompanied by anomalously warm sea surface temperatures (SSTs) over much of the Southern Ocean (Figures 1b and 2b). This episode was unanticipated given long-term trends of Antarctic sea ice increase and Southern Ocean surface cooling over recent decades [*Parkinson and Cavalieri*, 2012; *Meehl et al.*, 2016; *Armour et al.*, 2016; *Purich et al.*, 2016]. Key questions are thus: what atmospheric and oceanic conditions led to this unprecedented event and what does it portend for the future of Antarctic sea ice?

The long-term increase in Antarctic sea ice over recent decades has been suggested to have been driven, at least in part, by a positive trend in the Southern Annular Mode (SAM) due to ozone depletion over the late twentieth century [*Thompson and Solomon*, 2002; *Marshall et al.*, 2014; *Armour and Bitz*, 2015]. Observational support for this mechanism is found in the correlations between SAM, SST, and Antarctic sea ice on interannual and shorter time scales: a positive SAM drives cooling and sea ice expansion through enhanced Ekman advection of cold surface waters northward [*Thompson and Solomon*, 2002; *Hall and Visbeck*, 2002; *Sen Gupta and England*, 2006; *Ferreira et al.*, 2015; *Kostov et al.*, 2017]. Eventually—on longer time scales—this enhanced northward Ekman transport is expected to lead to upwelling of warmer subsurface waters from below the mixed layer and thus lead to sea ice decline [*Ferreira et al.*, 2015; *Kostov et al.*, 2017]. While the large-scale wind changes associated with SAM anomalies are primarily zonal, it has been shown that SAM changes also exhibit a nonannular component (especially in the Amundsen Sea Low region), and these meridional wind anomalies have been linked to sea ice changes [e.g., *Turner et al.*, 2009; *Holland and Kwok*, 2012; *Haumann et al.*, 2014]. An additional process that has been proposed to explain the long-term sea ice increase is enhanced freshwater flux from Antarctic ice shelf melt [*Bintanja et al.*, 2013]; however, it is unclear whether enhanced freshwater flux into the Southern Ocean could have driven a sea ice expansion as significant as the observed [*Swart and Fyfe*, 2013; *Pauling et al.*, 2016]. It is also possible that multidecadal variability of the ice-ocean system has contributed to the sea ice increase as well [e.g., *Polvani and Smith*, 2013].

Over the coming century, greenhouse gas (GHG) driven warming of the Southern Ocean, though muted relative to global mean warming [*Armour et al.*, 2016], is projected to eventually drive a slow decline in Antarctic

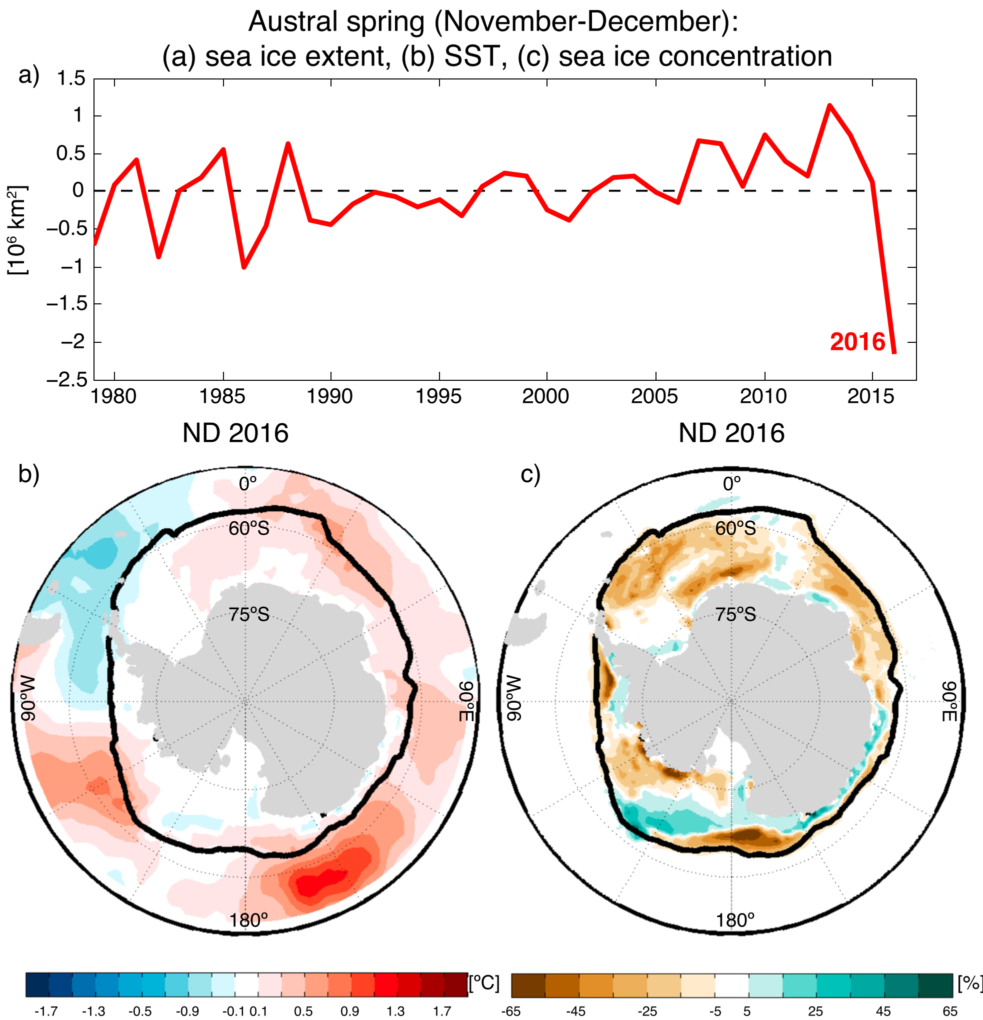

Figure 1. (a) Temporal evolution of Antarctic austral spring (November–December mean) anomalous sea ice extent (10^6 km^2). (b) Anomalous SST in ND2016 (°C) and (c) anomalous sea ice concentration (%) in ND2016. The sea ice extent (area with at least 15% sea ice concentration) is indicated by the solid black contour line.

sea ice [*Armour and Bitz*, 2015]. This long-term ice loss may also be enhanced by slow ozone recovery, to the extent that it induces SAM changes that reduce the anticipated trend toward more positive SAM associated with GHG forcing [*Thompson et al.*, 2011; *Smith et al.*, 2012]. In any case, abrupt changes in the Antarctic sea ice cover are not expected to be driven by slowly varying forcing [*Armour et al.*, 2011], suggesting that natural variability may have made a substantial contribution to the observed sea ice decline in austral spring 2016.

On interseasonal to decadal time scales, climate variability in the tropics has been shown to strongly affect the Antarctic sea ice cover [e.g., *Yuan*, 2004; *Turner*, 2004; *Stammerjohn et al.*, 2008; *Ding et al.*, 2011; *Simpkins et al.*, 2012; *Li et al.*, 2014; *Nuncio and Yuan*, 2015; *Meehl et al.*, 2016; *Purich et al.*, 2016; *Kohyama and Hartmann*, 2016], thus creating the potential for short-term changes to oppose long-term climate trends. However, the relative importance of different tropical climate modes—such as the El Niño–Southern Oscillation (ENSO) and the Indian Ocean Dipole (IOD)—and the spatial details and seasonal modulation of the different teleconnection patterns are all still areas of active research and debate. One pathway for ENSO to affect the SH high latitudes is via tropical forced atmospheric Rossby wave propagation [*Karoly*, 1989]—the so-called Pacific South America (PSA) pattern. These ENSO-induced extratropical teleconnections form an atmospheric bridge [*Lau and Nath*, 1996; *Li*, 2000; *Stuecker et al.*, 2015a], which enables ENSO to influence the remote extratropical oceans via anomalous heat and momentum fluxes. Indeed, it has been shown using slab ocean model experiments that

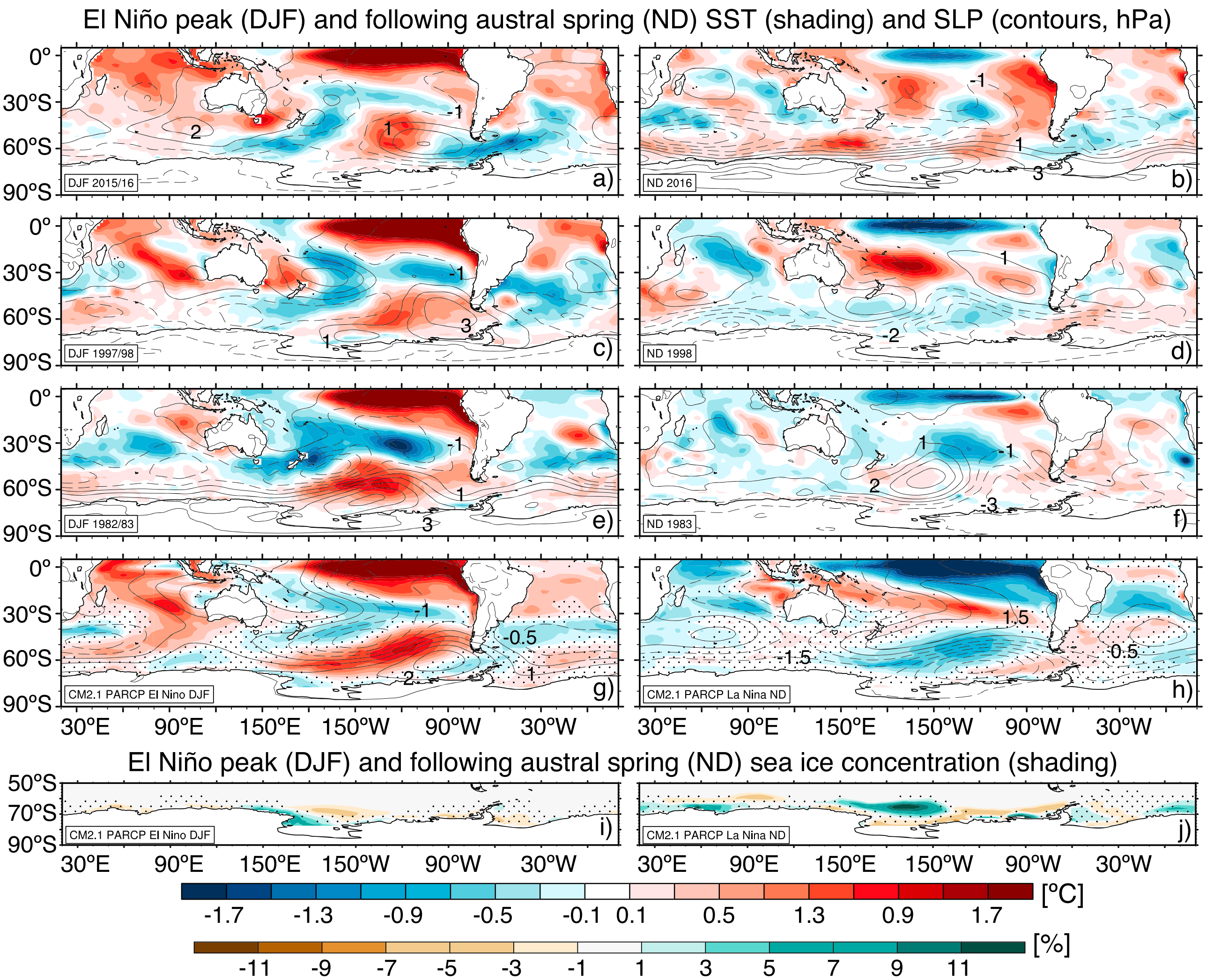

Figure 2. (a–f) Southern Hemisphere SST (shading, °C) and SLP (contours, hPa) anomalies for the peak time (December–February: DJF) of the three largest El Niño events and for the following austral spring season (November–December: ND). (g and h) Composite mean (n = 28) SST (shading, °C) and SLP (contours, hPa) anomalies for DJF El Niño (Figure 2g) and ND La Niña (Figure 2h) in the partially coupled (PARCP) sinusoidal CM2.1 experiment. (i and j) Composite mean (n = 28) sea ice concentration (shading, %) anomalies for DJF El Niño (Figure 2i) and ND La Niña (Figure 2j) in the PARCP sinusoidal CM2.1 experiment. Stippled areas indicate that the anomalous SST (Figures 2g and 2h) and sea ice concentrations (Figures 2i and 2j) are nonsignificantly different from zero at the 90% confidence level based on a two-tailed t test.

these teleconnections can affect Southern Ocean SSTs [*Li*, 2000], which could then initiate high-latitude air-sea coupled dynamics, for instance, via the Antarctic circumpolar wave mechanism [*White and Peterson*, 1996; *Cai and Baines*, 2001].

Recently, it has been shown that tropical forcing associated with the negative phase of the Interdecadal Pacific Oscillation (IPO) resulted in a deepening of the Amundsen Sea Low and corresponding local sea ice expansion in the eastern Ross and Amundsen Seas and a decrease in the Bellingshausen Sea [*Meehl et al.*, 2016; *Purich et al.*, 2016]—an Antarctic dipole [*Yuan and Martinson*, 2000] of sea ice concentration and SST anomalies. Moreover, decadal trends in central Pacific warming have been invoked to explain the recent warming over continental West Antarctica [*Ding et al.*, 2011]. In addition to zonally asymmetric Rossby wave propagation, ENSO can also influence the SH high latitudes via its relationship with the SAM [*L'Heureux and Thompson*, 2006; *Fogt and Bromwich*, 2006; *Stammerjohn et al.*, 2008; *Ding et al.*, 2012]. In the austral summer season, approximately 25% of temporal SAM variability can be attributed to tropical ENSO forcing [*L'Heureux and Thompson*, 2006]. However, it seems that the zonal location of the tropical ENSO forcing can cause differing impacts on the SAM [*Ding et al.*, 2012]. Further complicating this picture is the fact that the ENSO-SAM relationship appears to be nonstationary on decadal time scales, which might be due to internal SAM variability and/or external

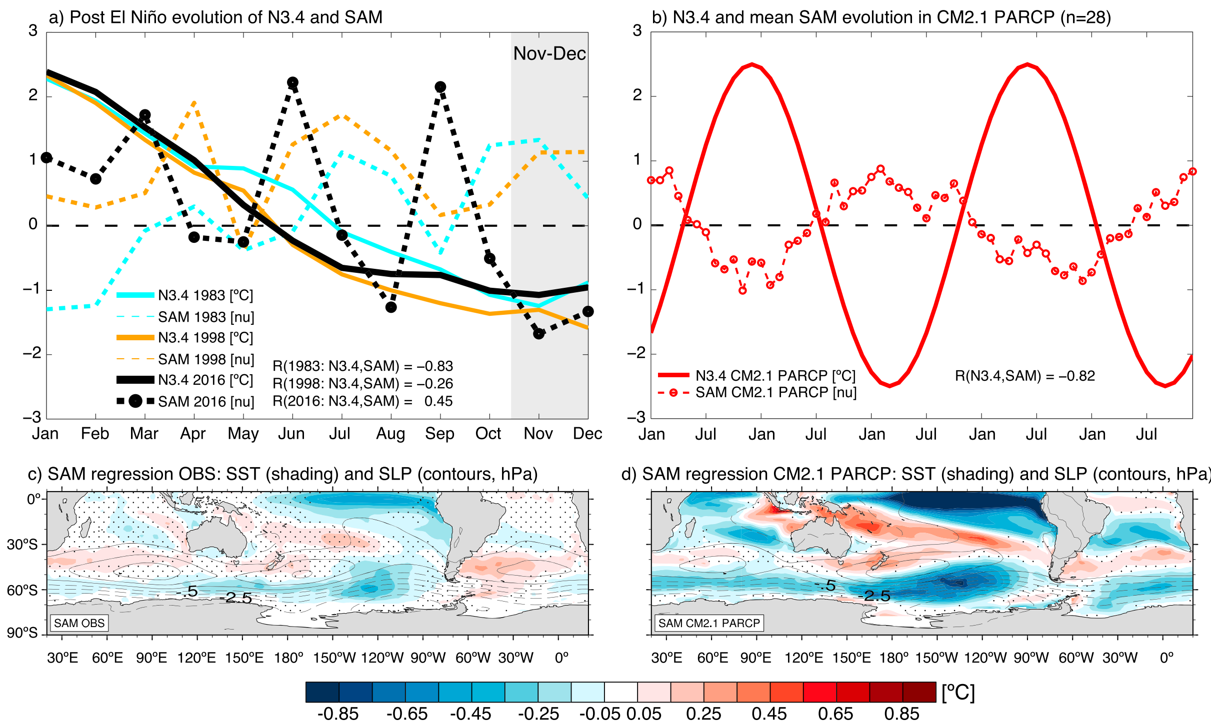

Figure 3. (a) Post El Niño year evolution of N3.4 (solid lines, °C) and normalized SAM indices (dashed lines, no units) for 2016 (black), 1998 (orange), and 1983 (cyan). The linear correlation coefficients between N3.4 and SAM for each of these years are given as insets. (b) N3.4 forcing (solid red line, °C) and composite mean ($n = 28$) normalized SAM index (dashed red line, no unit) for the partially coupled (PARCP) sinusoidal CM2.1 experiment. (c) Anomalous SST (°C) and SLP (contours, hPa) linear regression coefficients for the observed (1979–2016) normalized November–December average SAM index. (d) Anomalous SST (°C) and SLP (contours, hPa) linear regression coefficients for the CM.21 PARCP November–December average normalized SAM index. Stippled areas indicate that the anomalous SST regression coefficients (Figures 3c and 3d) are nonsignificantly different from zero at the 95% confidence level based on a two-tailed t test.

forcings such as ozone [*Fogt and Bromwich*, 2006]. An attribution of these processes is complicated by the fact that both SAM and PSA project on the Amundsen Sea Low circulation.

During austral summer 2015/2016 one of the largest El Niño events in the observational record occurred, which was followed by a weak La Niña that developed in austral winter-spring 2016. This raises the question of whether the aforementioned mechanisms involving ENSO played a role in the observed record low sea ice extent during austral spring 2016.

2. Observed Conditions Leading to 2016 Sea Ice Decline

In light of the above dynamical drivers of Antarctic sea ice variability, we next consider the large-scale atmospheric and oceanic conditions that set the stage for the unprecedented sea ice decline in austral spring of 2016. We focus specifically on the months leading up to and including November–December 2016 (ND2016), during which the record low 2016 austral spring and summer sea ice extent first became exceptionally pronounced. The previous austral summer season (2015/2016) was characterized by an extreme El Niño (Figures 2a and 3a), exhibiting anomalously warm SSTs in the central and eastern equatorial Pacific. The amplitude of the 2015/2016 El Niño was comparable to the two largest previous events in 1982/1983 and 1997/1998 (Figures 2c and 2e), and thus, we use those events as a reference against which to compare the evolution of atmospheric and oceanic conditions.

During their December–February (DJF) peak phase, each of these El Niño events exhibited an anomalous sea level pressure (SLP) pattern that resembled a PSA wave train originating from tropical diabatic forcing (Figures 2a, 2c, and 2e). These characteristic atmospheric circulation patterns were accompanied by SST anomalies across all SH oceanic basins (Figures 2a, 2c, and 2e) that were remarkably consistent (including anomalously warm SSTs within the eastern Ross and Amundsen Seas), suggesting an atmospheric bridge mechanism [*Lau and Nath*, 1996; *Li*, 2000] as a cause for some of this commonality. By the following austral

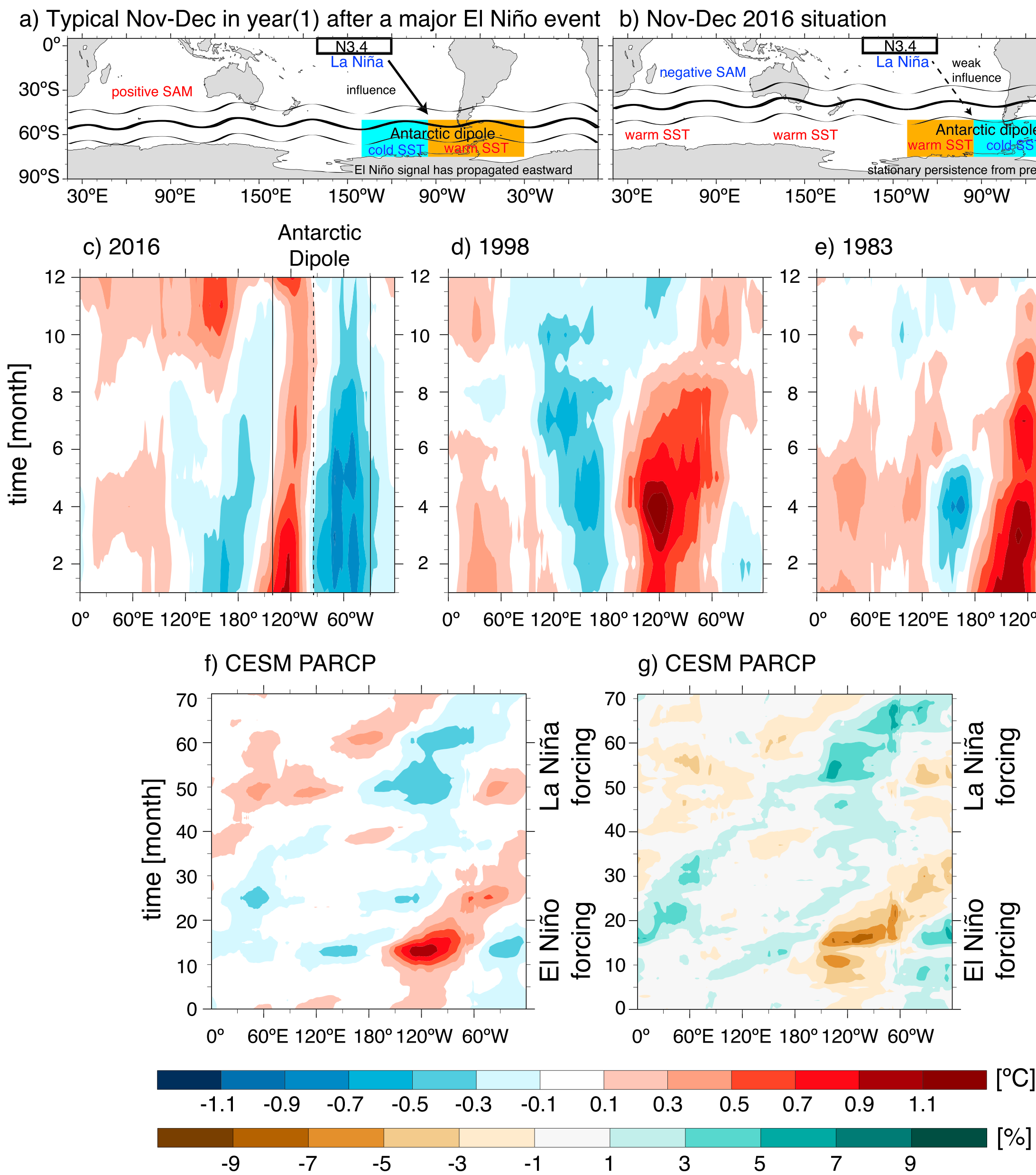

Figure 4. (a and b) Schematic of the results: Typical November–December situation in the year following a major El Niño event (Figure 4a). Atmospheric and oceanic conditions during November–December 2016 with El Niño-induced SST anomaly persistence in the Antarctic dipole region (orange and cyan boxes) and a northward shift of the jet stream and associated warm SST anomalies around Antarctica (negative SAM phase) (Figure 4b). (c–e) Hovmöller diagrams for the temporal evolution of anomalous SST in the Southern Ocean (averaged from 70°S to 50°S) for the decaying El Niño years 2016 (Figure 4c), 1998 (Figure 4d), and 1983 (Figure 4e). (f) The same but for the ensemble mean (n = 29) CESM1 PARCP experiment (Figure S2c). (g) Hovmöller diagram for the temporal evolution of sea ice concentration anomalies in the Southern Ocean (averaged from 70°S to 50°S) for the ensemble mean (n = 29) CESM1 PARCP experiment (Figure S2c).

spring seasons, La Niña conditions, characterized by anomalous cold SSTs in the central and eastern equatorial Pacific, were prevalent for all three events. Yet, importantly, the magnitude of La Niña was significantly smaller for ND2016 than for the ND1998 post El Niño austral spring season and of similar magnitude to the ND1983 La Niña (Figures 2b, 2d, and 2f). Sea ice concentration anomalies that are largely consistent with these SST anomalies also occurred (Figure S1 in the supporting information), which can be explained by the strong coupling between SST and sea ice concentrations. Therefore, remote tropical forcing that affects either SSTs or sea ice concentrations will initiate coupled feedback processes between these two variables. Here we mostly emphasize the SST anomalies because they extend beyond the sea ice edge and can be followed through the summer, when Antarctic sea ice extent is normally very low.

Another major difference between ND2016 and the other post El Niño austral springs is the phase of SAM: while ND1983 and ND1998 have a positive SAM and relatively cool (compared to ND2016) SSTs around Antarctica (as is typical for La Niña conditions), ND2016 exhibits an opposite pattern with negative SAM and warm SSTs over most of the Southern Ocean (Figures 2b, 2d, 2f, and 3a). In fact, the negative SAM during ND2016 well exceeded one standard deviation (Figure 3a).

From these results, it appears that differences between tropical forcing and SAM among these three events have contributed to their strikingly different SLP and SST patterns over the SH and thus their very different sea ice behaviors in the austral spring following the strong El Niños. We thus hypothesize that the unprecedented low sea ice extent in ND2016 arose from a confluence of rare atmospheric and oceanic conditions. In particular, anomalously warm SSTs within the eastern Ross and Amundsen Seas, generated by the preceding 2015/2016 El Niño, persisted strongly through ND2016, perhaps due to the relatively weak La Niña in that year. Additionally, a pronounced negative SAM anomaly in ND2016—the opposite from what is typical during La Niña, and thus likely due to internal variability—drove warming and sea ice decline around the rest of Antarctica in combination with other unforced atmospheric variability [*Turner et al.*, 2017]. These conditions, compared to those typical of a post strong El Niño year, are shown schematically in Figures 4a and 4b. In what follows, we turn to numerical general circulation model simulations to further illustrate these proposed mechanisms.

3. Simulating the Sea Ice Response to Major Modes of Climate Variability

To further investigate the respective roles of tropical ENSO forcing and internal SAM variability in shaping the ND2016 SH atmospheric circulation and SST patterns, we perform simulations with two coupled general circulation models. In the first experiment (using the CM2.1 model) [*Delworth et al.*, 2006], we prescribe a repeating cycle of ENSO—El Niño followed by La Niña—in the tropical eastern Pacific while allowing for full dynamical air-sea coupling everywhere else [*Stuecker et al.*, 2017] (an ensemble of 28 cycles; see section 5 and Figures S2a and S2b), allowing us to isolate and identify the anomalous SLP and SST response to tropical ENSO forcing over the Southern Ocean. Note that this model setup also allows us to capture the ENSO-induced climate variability in the other basins, such as the IOD [*Stuecker et al.*, 2017], which has been shown to also influence Antarctic climate variability [*Nuncio and Yuan*, 2015]. In the second experiment (using the CESM1 model) [*Gent et al.*, 2011], we add ENSO neutral years between El Niño and La Niña to investigate the persistence of El Niño-induced SST anomalies in the Southern Ocean (an ensemble of 29 cycles; see section 5 and Figures S2a and S2c). Here we focus mostly on the model-simulated SST signal given the close relationship between SSTs and sea ice concentrations seen in the observations (Figures 1b and 1c) [*Smith et al.*, 2008; *Comiso et al.*, 2017] and in model experiments [*Ferreira et al.*, 2015] and the fact that models usually exhibit smaller biases in simulating SST compared to sea ice concentrations.

First, we compare the model El Niño peak DJF ensemble mean response of the first experiment (Figures 2g, 2i, and S1g) with the three observed El Niño events (Figures 2a, 2c, and 2e). The model captures the atmospheric circulation and SST anomaly features remarkably well. Note that the simulated SST anomalies (Figure 2g) and sea ice concentration anomalies (Figures 2i and S1g) are highly negatively correlated poleward of 60°S (the centered spatial pattern correlation coefficient attains a value of −0.98 (significant at the 95% confidence level for 2 degrees of freedom) for the DJF peak ensemble mean response in areas where the model climatological sea ice concentrations are above 15%). Near Antarctica, the SST response is characterized by a pronounced zonal dipole structure between the eastern Ross and Amundsen Seas (positive) and the Bellingshausen Sea (negative; Figure 2g). This Antarctic dipole is part of a large-scale SST anomaly pattern in the southern Pacific. Additionally, we observe the tropical Indian Ocean basin warming [*Xie et al.*, 2009] together with a meridional SST anomaly dipole to the south of the African continent. Furthermore, a clear meridional tripole SST anomaly structure is evident in the Atlantic basin. In contrast, the ND La Niña composite (Figures 2h, 2j, and S1h) is characterized by nearly opposite patterns (again SST anomalies and sea ice concentration anomalies are highly negatively correlated poleward of 60°S with a centered spatial pattern correlation coefficient of −0.87 (significant at the 95% confidence level for 4 degrees of freedom) in areas where the model climatological sea ice concentrations are above 15%). Both the slightly different seasonality (ND versus DJF) and nonlinearities in ENSO-induced impacts [*Stuecker et al.*, 2015a, 2015b] might explain the small differences in the forced responses between DJF El Niño and ND La Niña. One of these seasonal differences is the ENSO-induced IOD signal in the tropical Indian Ocean that peaks right before the ND season [*Stuecker et al.*, 2017], which is subsequently replaced by basin-wide Indian Ocean warming in the DJF season.

Both ND1998 and ND1983 (Figures 2d and 2f) have a high similarity (ND1998 more than ND1983) with the model ND La Niña composite (Figure 2h), including the large-scale SST pattern and the positive phase of SAM. In contrast, ND2016 (Figure 2b) exhibits high-latitude SLP and SST features that resemble more the model El Niño pattern (Figure 2g). It comprises the El Niño-like zonal Antarctic SST anomaly dipole, a negative SAM, and anomalously warm SSTs in most other Antarctic sectors. Next we investigate the reason that during the 2016/2017 La Niña we observe an El Niño-like zonal Antarctic dipole together with a zonally quasi-symmetric warming around the rest of Antarctica in ND2016. Our hypothesis is that the relative contributions of (i) the absence of a strong quasi-instantaneous SH response to tropical La Niña forcing, (ii) a quasi-stationary persistence of Antarctic dipole SST anomalies induced by tropical El Niño forcing during the previous austral summer, and (iii) internal unforced SAM variability largely determined the ND2016 Southern Ocean SST and sea ice response. Next we explore the relative role of these processes for the observed ND2016 event.

3.1. The Antarctic SST Anomaly Dipole

Both the observations (Figures 2a, 2c, and 2e) and our CM2.1 model experiment (Figure 2g) demonstrate that a pronounced zonal Antarctic SST anomaly dipole is generated as part of the PSA and SAM response during the peak El Niño phase. Usually, this pattern reverses its sign in the following ND season (Figures 2d and 2h) due to (i) the SH atmospheric circulation forced by La Niña (Figure 2h), (ii) thermodynamic damping of the anomalies that were generated by the previous El Niño, and (iii) eastward advection of these SST anomalies by the mean zonal ocean surface currents [e.g., *White and Peterson*, 1996] (also see Figures 4c–4g).

The typical sign reversal of the Antarctic dipole due to these processes (i.e., in 1983 and 1998) is clearly captured by the first model experiment (CM2.1) during La Niña conditions (Figure 2h). In contrast, the unusual long persistence and quasi-stationary character of the El Niño Antarctic dipole pattern and of the SST anomalies in other regions during 2016 become even more evident in the month-to-month evolution of the observed SST anomalies and 850 hPa geopotential height (Z850) anomalies (Figure 5) and in a Hovmöller plot of Southern Ocean SSTs (Figure 4c). The Antarctic dipole shows the opposite phase in ND1998 (Figure 2d) and nearly no signature in ND1983 (Figure 2f), which clearly highlights the unusual persistence of this pattern in 2016 (Figures 2b, 4c, and 5). The unusual long persistence in 2016 appears to be due to a combination of (i) the quasi-stationary character of the anomalies and (ii) the smaller amplitude of the 2016 La Niña compared to the 1998 La Niña (Figure 3a). The El Niño-induced Antarctic dipole quickly decayed in both 1983 (Figure 4e) and 1998 (Figure 4d), likely due to a combination of the following processes: (i) thermodynamic damping, (ii) eastward advection of the anomalies as part of the Antarctic circumpolar wave, and (iii) vertical ocean mixing. The detailed atmospheric and oceanic conditions that led to this highly unusual quasi-stationary persistence throughout 2016 need to be addressed in a future study. However, we suggest that the lack of a large La Niña influence on the Southern Ocean in late 2016 enabled this persistence, given that a La Niña-forced SST response in the eastern Ross, Amundsen, and Bellingshausen Seas (Figure 2h) would be of opposite sign compared to what occurred in ND2016 (Figure 2b).

The effect of La Niña on the turnabout of the Antarctic dipole can be seen when comparing the two model experiments: When El Niño is followed by ENSO-neutral conditions (CESM1 experiment), we observe the persistence of an SST anomaly dipole pattern (and corresponding sea ice concentration anomaly dipole) that has been thermodynamically damped and simultaneously advected eastward by the mean zonal surface ocean currents (Figures 4f and 4g), resulting in an opposite phase of the dipole in the original regions (Figure S3). The effect of La Niña (CM2.1 experiment) then further amplifies this pattern (Figure 2h). Importantly, the CESM1 model experiment well captures the ENSO-forced Antarctic circumpolar wave that is forced twice during each 6 year experiment cycle (during El Niño and La Niña) and propagates around Antarctica approximately with the same period as the experiment cycle (Figures 4f and 4g). Note that some model differences exist in the simulated Southern Ocean SST response to a DJF El Niño forcing between CM2.1 (Figure 2g) and CESM1 (Figure S3) outside the Antarctic dipole regions.

The large amplitude of the ND1998 La Niña exhibits a SH response (Figure 2d) that is very similar to the model ND La Niña composite (Figure 2h). In contrast, the ND2016 La Niña had a weaker amplitude during the austral spring season (Figure 3a). It thus appears that the unique SST pattern in the Antarctic dipole sectors during ND2016 can be partly understood as arising from a combination of a strong El Niño followed by a relatively

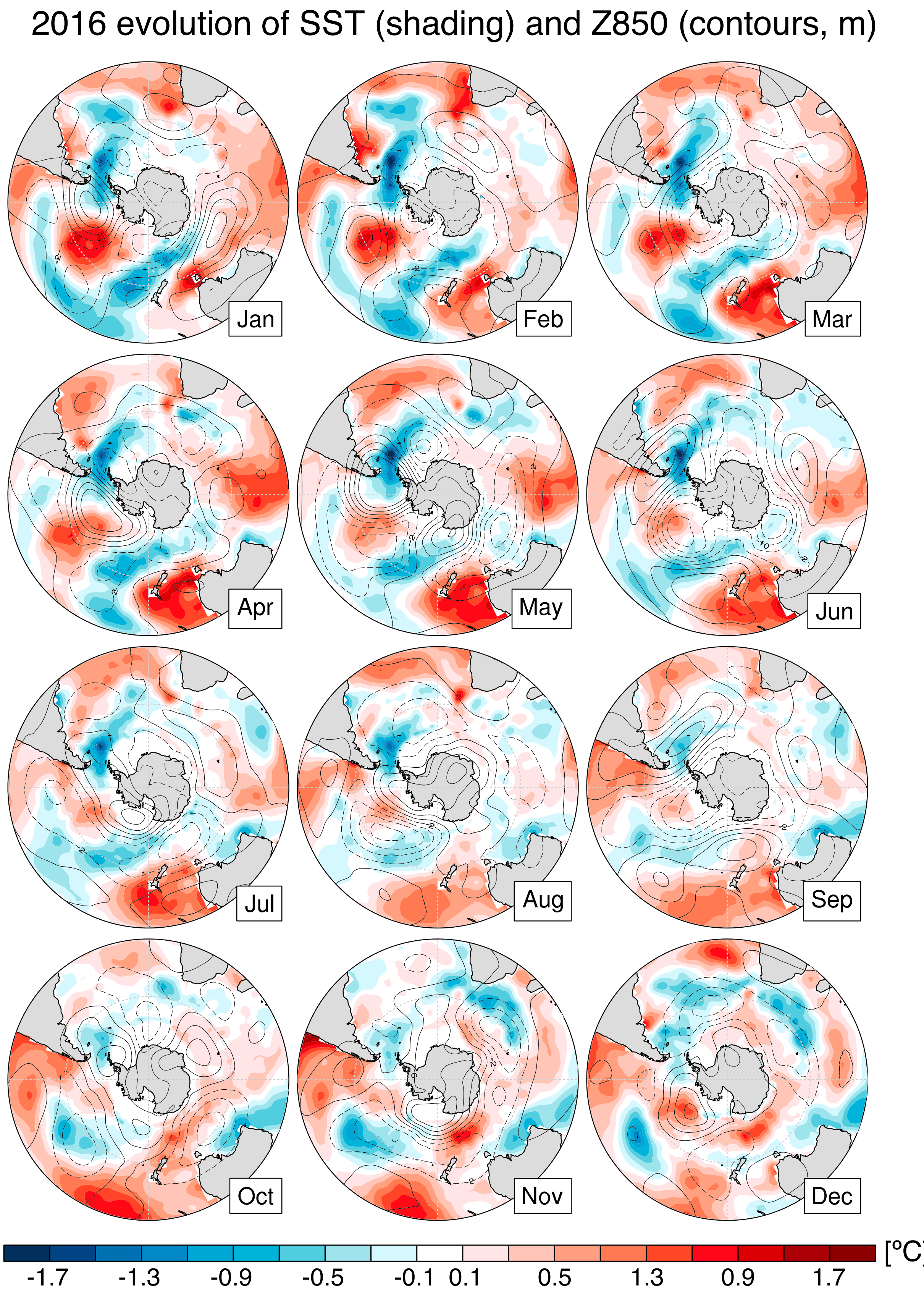

Figure 5. Monthly temporal evolution of the 2016 anomalous SST (shading, °C) and 850 hPa geopotential height (contours from −14 to 14 by 4, m).

weak La Niña. Next we will examine whether some remaining features of ND2016, particularly the warming around the rest of the Antarctica, can be understood in terms of a differing phase of SAM in ND2016 relative to ND1998 and ND1983.

3.2. The Southern Annular Mode

The anomalous SST and SLP regression patterns associated with the SAM agree well between the observations (Figure 3c) and the CM2.1 model experiment (Figure 3d), thereby giving us confidence that essential SAM dynamics and their relationship with ENSO are well captured by this model. Note that these SAM patterns also project weakly on the Amundsen Sea Low and the Antarctic dipole SST anomaly dipole. When minimizing internal unforced variability by calculating the model ensemble mean response to the ENSO forcing, we find that the SAM index is highly anticorrelated ($R = -0.82$, statistically significant at the 99% level) with the ENSO forcing (Figure 3b). This highly negative correlation between ENSO forcing and SAM demonstrates that the linear ENSO signal dominates the SAM response in this particular model and that nonlinear ENSO-induced high-frequency variability [*Stuecker et al.*, 2015b] likely plays only a second-order role for the simulated SAM (note that while ENSO explains part of the SAM variance, it is unforced internal variability that dominates SAM variability in the observations) [e.g., *L'Heureux and Thompson*, 2006].

Both the observations (Figures 3a and 3c) and the simulation (Figures 3b and 3d) show that La Niña events are usually associated with a positive SAM; therefore, we suggest that the negative SAM during ND2016 arose from internal atmospheric variability. In turn, the strongly negative SAM during ND2016 potentially further contributed to warm SSTs and sea ice decline around Antarctica and in the eastern Ross and Amundsen Seas (Figures 3a, 3c, and 4b). We emphasize that positive ice-ocean feedback processes are likely important. For instance, negative sea ice anomalies can result in positive SST anomalies, which then would favor further sea ice decline.

3.3. Analogue Events in CMIP5

To quantify the uniqueness of the ND2016 sea ice event, we use preindustrial control experiments from 25 models from the CMIP5 archive and search for analogue events. Our criterium is similarity to the observed 2016 climate conditions: a strong El Niño needs to be followed by only a moderate La Niña with large negative SAM in these model simulations to qualify as an analogue event (see section 5). This combination occurs on 121 occasions in $\sim$13,000 model years. As an example we show the four of these events that exist in the Norwegian Earth System Model Version 1-M (NorESM1-M) [*Bentsen et al.*, 2013] preindustrial control experiment, of which two have well below negative 1×10^6 km^2 sea ice extent anomalies (Figure S4). This shows that our mechanism can, in principle, generate large enough sea ice concentration anomalies that together with internal sea ice variability could explain the ND2016 event.

4. Summary and Conclusions

We conclude that two main factors contributed to the extreme low sea ice extent during ND2016 (Figures 1a and 1c). First, the extreme 2015/2016 El Niño-induced SST anomalies in the eastern Ross, Amundsen, and Bellingshausen Seas that remained quasi-stationary and persisted through ND2016 (Figures 4c and 5), allowed by an usually weak La Niña. Second, a strongly negative SAM phase in ND2016 (opposite to what is normally expected for a La Niña, and thus likely due to internal unforced atmospheric variability) resulted in anomalous warming in the Southern Ocean and was thus conducive to the extreme low sea ice extent (Figures 3a and 3c), which is supported by our CM2.1 model experiment (Figures 3b and 3d). The strongly negative SAM phase in ND2016 was also seen in Antarctic station-based observations [*Turner et al.*, 2017]. Hence, the ND2016 warming pattern (Figures 1b and 2b) can be seen as a combination of two rare factors, which is exemplified by the exceptional character of this event. A summary of these mechanisms is shown as a schematic in Figures 4a and 4b. Our results suggest that atmospheric and oceanic conditions drove a significant part of the evolution of large-scale SST and sea ice concentration anomalies in 2016, likely aided by coupled feedbacks between sea ice and the ocean. Given the extreme negative anomalies of this event, it is possible that unforced sea ice variability was a further important contributor.

Furthermore, our results demonstrate that some of the Southern Hemisphere SST and SLP features associated with a negative IPO phase [*Purich et al.*, 2016, Figure 1] also emerge on interannual time scales for La Niña conditions (Figure 2h). For instance, both a negative IPO phase and La Niña conditions force a positive SAM response and a deepening of the Amundsen Sea Low, corresponding to anomalous cooling along Antarctica except the Bellingshausen Sea region (Figures 3c and 3d). Previous research demonstrated that the persistence and reemergence of Southern Ocean SST anomaly patterns generate predictability for Antarctic sea ice [e.g., *Holland et al.*, 2013]. Our results confirm that tropical climate variability should provide a predictable component for Southern Hemisphere sea ice area and extent on seasonal to interannual time scales, despite pronounced unforced (and thus unpredictable on time scales beyond weather forecasting) internal variability in this region. Future occurrences of similar extreme events should be rare given the required combination of mechanisms; however, they cannot be ruled out given the existence of pronounced internal climate variability in both the tropics and high latitudes. Thus, we expect Antarctic sea ice to regress to the long-term trend in the near future.

5. Methods

We use the Extended Reconstructed Sea Surface Temperature (ERSST) v3b [*Smith et al.*, 2008] data set for SSTs and the Japanese 55 year Reanalysis [*Kobayashi et al.*, 2015] for SLP and 850 hPa geopotential height (Z850). The anomalous November–December SH sea ice extent is obtained from the NSIDC (National Snow and Ice Data Center) sea ice index version 2 [*Fetterer et al.*, 2016]. The sea ice concentration for ND2016 is the daily near-real-time DMSP Special Sensor Microwave Imager Sounder (SSMIS) passive microwave product product [*Cavalieri et al.*, 1996]. Anomalies were computed with respect to the climatology from the DMSP SSM/I-SSMIS product [*Maslanik and Stroeve*, 1999]. All anomalies are respective to the 1979–2016 climatology.

The Niño3.4 (N3.4) index is used to characterize ENSO variability. It is defined as the area-averaged SST anomalies from 170°W to 120°W and 5°S to 5°N. The SAM index is defined as the normalized first principal component (PC1) of the anomalous monthly Z850 in the extratropical Southern Hemisphere (20°S–90°S) [*Thompson and Wallace*, 2000] for both the observations (explaining 25.3% of the variance) and model experiment (explaining 20.0% of the variance).

We use the GFDL CM2.1 [*Delworth et al.*, 2006] coupled global climate model to conduct a partially coupled (PARCP) experiment for which a 2.5 year sinusoidal ENSO SST forcing is prescribed in the tropical eastern Pacific with a damping time scale of 5 days [*Stuecker et al.*, 2017]. Outside of this forcing region the atmosphere, ocean, and sea ice are fully coupled (Figure S2a). The atmosphere and ocean components are general circulation models, which along with the thermodynamic-dynamic sea ice model capture high-latitude ocean-atmosphere-ice interactions. The model is integrated for 140 years and 5 year cycles are composited ($n = 28$). A sinusoidal forcing is chosen (Figure S2b) because in this case we are able to clearly identify both the linear and nonlinear impacts of ENSO [*Stuecker et al.*, 2015b, 2017]. Further details on the CM2.1 PARCP experimental setup are given in *Stuecker et al.* [2017]. Importantly, this experimental setup allows us to diagnose the remote impacts of tropical ENSO forcing while allowing for extratropical ocean-atmosphere-ice coupled dynamics.

We use a second global climate model—CESM 1.2.0 [*Gent et al.*, 2011] with the CAM4 [*Neale et al.*, 2013] atmospheric component (nominally 2° horizontal resolution for the atmosphere and 1° for the ocean and sea ice)—to conduct a similar PARCP experiment (same forcing region and damping time scale as in the CM2.1 experiment; Figure S2a). The only difference is the time evolution of the forcing, which is chosen so that ENSO-neutral conditions persist for over a year after each El Niño and La Niña event (Figure S2c). This allows us to estimate the persistence of El Niño-induced Southern Ocean SSTs if no La Niña would follow immediately—and vice versa (Figure S2c). The CESM1 PARCP experiment is integrated for 174 years, and 6 years cycles are composited ($n = 29$).

To investigate the uniqueness of the ND2016 sea ice event, we use 25 model preindustrial control experiments from the CMIP5 archive and search for analogue events. The criteria that need to be fulfilled to qualify as an analogue are the following: (i) A large El Niño event (January–March amplitude above the 90th percentile) occurred, (ii) no large La Niña followed (N3.4 no lower than −0.5°C in October–December (OND)) by the end of the same year, and (iii) the OND SAM following the El Niño is below one model standard deviation.

Acknowledgments
This research was supported by the NOAA Climate and Global Change Postdoctoral Fellowship Program, administered by UCAR's Cooperative Programs for the Advancement of Earth System Sciences (CPAESS) and with funding from the National Science Foundation through grants PLR-1341497 and PLR-1643431. We thank two reviewers for their helpful comments. We acknowledge the World Climate Research Programme's Working Group on Coupled Modelling, which is responsible for CMIP, and we thank the climate modeling groups for producing and making available their model output. For CMIP the U.S. Department of Energy's Program for Climate Model Diagnosis and Intercomparison provides coordinating support and led development of software infrastructure in partnership with the Global Organization for Earth System Science Portals. The model experiment output can be obtained from the corresponding author. The model code to reproduce these experiments can be obtained from https://github.com/mom-ocean/MOM4p1 and http://www.cesm.ucar.edu/models/cesm1.2/. The observational and reanalysis data used in this study can be obtained from https://www1.ncdc.noaa.gov/pub/data/cmb/ersst/v3b/netcdf/, http://jra.kishou.go.jp/JRA-55/, and https://nsidc.org/data.

References

Armour, K. C., and C. M. Bitz (2015), Observed and projected trends in Antarctic sea ice, *US Clivar Variations*, *13*, 12–19.
Armour, K. C., I. Eisenman, E. Blanchard-Wrigglesworth, K. E. McCusker, and C. M. Bitz (2011), The reversibility of sea ice loss in a state-of-the-art climate model, *Geophys. Res. Lett.*, *38*, L16705, doi:10.1029/2011GL048739.
Armour, K. C., J. Marshall, J. Scott, A. Donohoe, and E. R. Newsom (2016), Southern Ocean warming delayed by circumpolar upwelling and equatorward transport, *Nat. Geosci.*, *9*, 549–554, doi:10.1038/ngeo2731.

Bentsen, M., et al. (2013), The Norwegian Earth System Model, NorESM1-M — Part 1: Description and basic evaluation of the physical climate, *Geosci. Model Dev.*, *6*, 687–720, doi:doi:10.5194/gmd-6-687-2013.

Bintanja, G., G. J. van Oldenborgh, S. S. Drijfhout, B. Wouters, and C. A. Katsman (2013), Important role for ocean warming and increased ice-shelf melt in Antarctic sea-ice expansion, *Nat. Geosci.*, *6*, 376–379, doi:10.1038/ngeo1767.

Cai, W., and P. G. Baines (2001), Forcing of the Antarctic Circumpolar Wave by El Niño–Southern Oscillation teleconnections, *J. Geophys. Res.*, *106*, 9019–9038, doi:10.1029/2000JC000590.

Cavalieri, D. J., C. L. Parkinson, P. Gloersen, and H. J. Zwally (1996), *Updated Daily. Sea Ice Concentrations From Nimbus-7 SMMR and DMSP SSM/I-SSMIS Passive Microwave Data, Version 1. 1*, NASA DAAC at the Natl. Snow and Ice Data Cent., Boulder, Colo., doi:10.5067/8GQ8LZQVL0VL. [Accessed 5 Jan 2017].

Comiso, J. C., R. A. Gersten, L. V. Stock, J. Turner, G. J. Perez, and K. Cho (2017), Positive trend in the antarctic sea ice cover and associated changes in surface temperature, *J. Clim.*, *30*, 2251–2267, doi:10.1175/JCLI-D-16-0408.1.

Delworth, T. L., et al. (2006), GFDL's CM2 global coupled climate models. Part I: Formulation and simulation characteristics, *J. Clim.*, *19*, 634–674, doi:10.1175/JCLI3629.1.

Ding, Q., E. J. Steig, D. S. Battisti, and M. Küttel (2011), Winter warming in West Antarctica caused by central tropical Pacific warming, *Nature Geosci.*, *4*, 398–403, doi:10.1038/ngeo1129.

Ding, Q., E. J. Steig, D. S. Battisti, and J. M. Wallace (2012), Influence of the tropics on the Southern Annular Mode, *J. Clim.*, *25*, 6330–6348, doi:10.1175/JCLI-D-11-00523.1.

Ferreira, D., J. Marshall, C. M. Bitz, S. Solomon, and A. Plumb (2015), Antarctic ocean and sea ice response to ozone depletion: A two-time-scale problem, *J. Clim.*, *28*, 1206–1226, doi:10.1175/JCLI-D-14-00313.1.

Fetterer, F., K. Knowles, W. Meier, and M. Savoie (2016), *Updated Daily. Sea Ice Index, Version 2.*, NSIDC: Natl. Snow and Ice Data Cent., Boulder, Colo., doi:10.7265/N5736NV7.

Fogt, R. L., and D. H. Bromwich (2006), Decadal variability of the ENSO teleconnection to the high-latitude South Pacific governed by coupling with the Southern Annular Mode, *J. Clim.*, *19*, 979–997.

Gent, P. R., et al. (2011), The community climate system model version 4, *J. Clim.*, *24*, 4973–4991, doi:10.1175/2011JCLI4083.1.

Hall, A., and M. Visbeck (2002), Synchronous variability in the Southern Hemisphere atmosphere, sea ice, and ocean resulting from the annular mode, *J. Clim.*, *15*, 3043–3057.

Haumann, F. A., D. Notz, and H. Schmidt (2014), Anthropogenic influence on recent circulation-driven Antarctic sea ice changes, *Geophys. Res. Lett.*, *41*, 8429–8437, doi:10.1002/2014GL061659.

Holland, P. R., and R. Kwok (2012), Wind-driven trends in Antarctic sea-ice drift, *Nat. Geosci.*, *5*, 872–875, doi:10.1038/ngeo1627.

Holland, M. M., E. Blanchard-Wrigglesworth, J. Kay, and S. Vavrus (2013), Initial-value predictability of Antarctic sea ice in the Community Climate System Model 3, *Geophys. Res. Lett.*, *40*, 2121–2124, doi:10.1002/grl.50410.

Karoly, D. J. (1989), Southern Hemisphere circulation features associated with El Niño–Southern Oscillation events, *J. Clim.*, *2*, 1239–1252.

Kobayashi, S., et al. (2015), The JRA-55 reanalysis: General specifications and basic characteristics, *J. Meteorol. Soc. Jpn.*, *93*(1), 5–48, doi:10.2151/jmsj.2015-001.

Kohyama, T., and D. L. Hartmann (2016), Antarctic sea ice response to weather and climate modes of variability, *J. Clim.*, *29*, 721–741, doi:10.1175/JCLI-D-15-0301.1.

Kostov, Y., J. Marshall, U. Hausmann, K. C. Armour, D. Ferreira, and M. M. Holland (2017), Fast and slow responses of Southern Ocean sea surface temperature to SAM in coupled climate models, *Clim. Dyn.*, *48*, 1595–1609, doi:10.1007/s00382-016-3162-z.

Lau, N.-C., and M. J. Nath (1996), The role of the "Atmospheric Bridge" in linking tropical pacific ENSO events to extratropical SST anomalies, *J. Clim.*, *9*, 2036–2057.

L'Heureux, M. L., and D. W. J. Thompson (2006), Observed relationships between the El Niño–Southern Oscillation and the extratropical zonal-mean circulation, *J. Clim.*, *19*, 276–287.

Li, Z. X. (2000), Influence of tropical Pacific El Niño on the SST of the Southern Ocean through atmospheric bridge, *Geophys. Res. Lett.*, *27*, 3505–3508, doi:10.1029/1999GL01182.

Li, X., D. M. Holland, E. P. Gerber, and C. Yoo (2014), Impacts of the North and tropical Atlantic Ocean on the Antarctic Peninsula and sea ice, *Nature*, *505*, 538–542, doi:10.1038/nature12945.

Marshall, J., K. C. Armour, J. R. Scott, Y. Kostov, U. Hausmann, D. Ferreira, T. G. Shepherd, and C. M. Bitz (2014), The ocean's role in polar climate change: Asymmetric Arctic and Antarctic responses to greenhouse gas and ozone forcing, *Phil. Trans. R. Soc. A*, *372*, doi:10.1098/rsta.2013.0040.

Maslanik, J., and J. Stroeve (1999), *Updated Daily. Near-Real-Time DMSP SSMIS Daily Polar Gridded Sea Ice Concentrations, Version 1*, NASA Natl. Snow and Ice Data Cent. Distributed Active Archive Center, Boulder, Colo., doi:10.5067/U8C09DWVX9LM. [Accessed 5 Jan 2017].

Meehl, G. A., J. M. Arblaster, C. M. Bitz, C. T. Y. Chung, and H. Teng (2016), Antarctic sea-ice expansion between 2000 and 2014 driven by tropical Pacific decadal climate variability, *Nat. Geosci.*, *9*, 590–595 doi:10.1038/ngeo2751.

Neale, R. B., J. Richter, S. Park, P. H. Lauritzen, S. J. Vavrus, P. J. Rasch, and M. Zhang (2013), The mean climate of the community atmosphere model (CAM4) in forced SST and fully coupled experiments, *J. Clim.*, *26*(14), 5150–5168, doi:10.1175/JCLI-D-12-00236.1.

Nuncio, M., and X. Yuan (2015), The influence of the Indian Ocean dipole on Antarctic sea ice, *J. Clim.*, *28*, 2682–2690, doi:10.1175/JCLI-D-14-00390.1.

Parkinson, C., and D. J. Cavalieri (2012), Antarctic sea ice variability and trends, 1979–2010, *The Cryosphere*, *6*, 871–880, doi:10.5194/tc-6-871-2012.

Pauling, A. G., C. M. Bitz, I. J. Smith, and P. J. Langhorne (2016), The response of the southern ocean and antarctic sea ice to freshwater from ice shelves in an Earth system model, *J. Clim.*, *29*, 1655–1672, doi:10.1175/JCLI-D-15-0501.1.

Polvani, L. M., and K. L. Smith (2013), Can natural variability explain observed Antarctic sea ice trends? New modeling evidence from CMIP5, *Geophys. Res. Lett.*, *40*, 3195–3199, doi:10.1002/grl.50578.

Purich, A., M. England, W. Cai, Y. Chikamoto, A. Timmermann, J. Fyfe, L. Frankcombe, G. Meehl, and J. Arblaster (2016), Tropical Pacific SST drivers of recent Antarctic sea ice trends, *J. Clim.*, *29*, 8931–8948, doi:10.1175/JCLI-D-16-0440.1.

Sen Gupta, A., and M. H. England (2006), Coupled ocean-atmosphere-ice response to variations in the Southern Annular Mode, *J. Clim.*, *19*, 4457–4486, doi:10.1175/JCLI3843.1.

Simpkins, G. R., L. M. Ciasto, D. W. J. Thompson, and M. H. England (2012), Seasonal relationships between large-scale climate variability and antarctic sea ice concentration, *J. Clim.*, *25*, 5451–5469, doi:10.1175/JCLI-D-11-00367.1.

Smith, K. L., L. M. Polvani, and D. R. Marsh (2012), Mitigation of 21st century Antarctic sea ice loss by stratospheric ozone recovery, *Geophys. Res. Lett.*, *39*, L20701, doi:10.1029/2012GL053325.

Smith, T. M., R. W. Reynolds, T. C. Peterson, and J. Lawrimore (2008), Improvements to NOAA's historical merged land-ocean surface temperature analysis (1880–2006), *J. Clim.*, *21*, 2283–2296.

Stammerjohn, S. E., D. G. Martinson, R. C. Smith, and X. Yuan (2008), Trends in Antarctic annual sea ice retreat and advance and their relation to El Niño-Southern Oscillation and Southern Annular Mode variability, *J. Geophys. Res.*, *113*, C03S90, doi:10.1029/2007JC004269.

Stuecker, M. F., F.-F. Jin, A. Timmermann, and S. McGregor (2015a), Combination mode dynamics of the anomalous northwest Pacific anticyclone, *J. Clim.*, *28*, 1093–1111, doi:10.1175/JCLI-D-14-00225.1.

Stuecker, M. F., F.-F. Jin, and A. Timmermann (2015b), El Niño–Southern Oscillation frequency cascade, *Proc. Natl. Acad. Sci. U.S.A.*, *112*, 13,490–13,495, doi:10.1073/pnas.1508622112.

Stuecker, M. F., A. Timmermann, F.-F. Jin, Y. Chikamoto, W. Zhang, A. T. Wittenberg, E. Widiasih, and S. Zhao (2017), Revisiting ENSO/Indian Ocean dipole phase relationships, *Geophys. Res. Lett.*, *44*, doi:10.1002/2016GL072308.

Swart, N. C., and J. C. Fyfe (2013), The influence of recent Antarctic ice sheet retreat on simulated sea ice trends, *Geophys. Res. Lett.*, *40*, 4328–4332, doi:doi:10.1002/grl.50820.

Thompson, D. W. J., and J. M. Wallace (2000), Annular modes in the extratropical circulation. Part I: Month-to-month variability, *J. Clim.*, *13*, 1000–1016.

Thompson, D. W. J., and S. Solomon (2002), Interpretation of recent Southern Hemisphere climate change, *Science*, *296*, 895–899, doi:10.1126/science.1069270.

Thompson, D. W. J., S. Solomon, P. J. Kushner, M. H. England, K. M. Grise, and D. J. Karoly (2011), Signatures of the Antarctic ozone hole in Southern Hemisphere surface climate change, *Nat. Geosci.*, *4*, 741–749, doi:10.1038/ngeo1296.

Turner, J. (2004), The El Niño-Southern Oscillation and Antarctica, *Int. J. Climatol.*, *24*, 1–31.

Turner, J., J. C. Comiso, G. J. Marshall, T. A. Lachlan-Cope, T. Bracegirdle, T. Maksym, M. P. Meredith, Z. Wang, and A. Orr (2009), Non-annular atmospheric circulation change induced by stratospheric ozone depletion and its role in the recent increase of Antarctic sea ice extent, *Geophys. Res. Lett.*, *36*, L08502, doi:10.1029/2009GL037524.

Turner, J., T. Phillips, G. J. Marshall, J. S. Hosking, J. O. Pope, T. J. Bracegirdle, and P. Deb (2017), Unprecedented springtime retreat of Antarctic sea ice in 2016, *Geophys. Res. Lett.*, *44*, 6868–6875, doi:10.1002/2017GL073656.

White, W. B., and R. G. Peterson (1996), An Antarctic circumpolar wave in surface pressure, wind, temperature and sea-ice extent, *Nature*, *380*, 699–702, doi:10.1038/380699a0.

Xie, S.-P., K. Hu, J. Hafner, H. Tokinaga, Y. Du, G. Huang, and T. Sampe (2009), Indian Ocean capacitor effect on Indo–western Pacific climate during the summer following El Niño, *J. Clim.*, *22*, 730–747, doi:10.1175/2008JCLI2544.1.

Yuan, X. (2004), ENSO-related impacts on Antarctic sea ice: A synthesis of phenomenon and mechanisms, *Antarctic Sci.*, *16*, 415–425, doi:10.1017/S0954102004002238.

Yuan, X., and D. G. Martinson (2000), Antarctic sea ice extent variability and its global connectivity, *J. Clim.*, *13*, 1697–1717.